Isospin effects in antinucleon-nucleon scattering and annihilation

P. Bydzovsky and R. Mach
Institute of Nuclear Physics, 25068 Rez, Czechoslovakia

F. Nichitiu
Nuclear Research Institute, Bucharest, Romania
(Received 12 June 1990)

Isospin effects in $N\bar{N}$ scattering and annihilation are studied here using the optical model. Real part of the effective $N\bar{N}$ potential was chosen to be the G-parity-transformed Bonn NN potential (OBEPQ). Parameters of the imaginary part of the optical potential were obtained by fitting the total $p\bar{p}\to p\bar{p}$, $p\bar{p}\to n\bar{n}$, and $\bar{n}p\to\bar{n}p$ cross sections to averaged experimental data represented here by analytical formulas. The model reproduces reasonably well the differential and total cross sections of $N\bar{N}$ scattering and charge-exchange reactions as well as the characteristics of $\bar{p}$ atoms. There is no evident relationship between the peculiar behavior of the real-to-imaginary ratio of the $p\bar{p}$ forward elastic scattering amplitude and isospin effects.

I. INTRODUCTION

The study of antiproton reactions has been greatly advanced by the LEAR facility, and an increasing body of experimental data is now available on antinucleon-nucleon scattering and annihilation in the low-energy region. The data on polarization observables in $N\bar{N}$ reactions are very scarce; therefore, a full scale phase-shift analysis cannot be done at present. However, recent measurements of elastic and total cross sections for $\bar{p}p\to\bar{p}p$ and $\bar{n}p\to\bar{n}p$ reactions along with the data for $\bar{p}p\to\bar{n}n$ charge exchange make it possible to gain some insight into the isospin content of the $N\bar{N}$ dynamics and first of all to extract some information of the $N\bar{N}$ annihilation strength in different isospin channels. This is the main objective of the present paper.

In the most ambitious calculations, at least some of the large number of meson states, which appear as a result of $N\bar{N}$ annihilation, are treated on the same footing as the scattering channels via the coupled channel formalism.[1] Such elaborate calculations, being now in their initial stage of development, can hardly serve as a basis for $\bar{N}$-nucleus calculations in the near future. Having in mind such applications, we report here on our optical model study, in which the Bonn potential for the NN interaction is used as a starting point. The G-parity-transformed Bonn potential (OBEPQ) serves as a real part of the optical potential pertinent to the $N\bar{N}$ system. The loss of flux from the elastic channel due to the annihilation is represented by the imaginary part of the optical potential. A phenomenological, volumelike form of the latter was chosen with room left for a possible isospin dependence of the annihilation process. The parameters of the absorption part of the optical potential have been obtained from the fit to the $\bar{p}p\to\bar{p}p$, $\bar{p}p\to\bar{n}n$, and $\bar{n}p\to\bar{n}p$ experimental data. The proton-neutron mass difference was taken into account in our calculations via the coupled-channel formalism. Therefore, the charge-exchange reaction $\bar{p}p\to\bar{n}n$ starts at a correct threshold value.

Earlier optical model studies Refs. 2–8 were done mostly in coordinate space, since the numerical techniques are very well developed there. However, microscopically constructed (optical) potential usually contain nonlocalities and velocity-dependent terms associated with the exchange of various mesons. Those features of the theory can be treated in coordinate space in a very crude way only by adopting rather severe simplifying assumptions. This is the reason why we work in momentum space and examine the extent to which the current momentum space techniques are applicable to the case of the $N\bar{N}$ reaction.

Some conclusions concerning the strength of $N\bar{N}$ annihilation in either isospin channel ($I=0,1$) have also been reached in earlier optical model work.[7] However, the $\bar{n}p\to\bar{n}p$ data were not available at that time. Other pieces of evidence have recently been collected in Refs. 9 and 10 indicating a rather important role of isospin effects in $N\bar{N}$ annihilation. The observables under consideration were the $\bar{p}$-nucleus annihilation cross sections in the case of $A=2$, 3, and 4 nuclei[9] and branching ratios of some exclusive annihilation channels.[10] Nevertheless, our understanding of isospin effects in $N\bar{N}$ annihilation is far from being satisfactory even on a phenomenological level.

A part of our work is the parametrization of experimental total, annihilation, and integrated differential cross sections for $\bar{p}p\to\bar{p}p$, $\bar{p}p\to\bar{n}n$, and $\bar{n}p\to\bar{n}p$ channels in terms of simple rational functions. The parametrization, presented in Sec. II, allows one to draw some conclusions about the mutual consistency of different experimental data and makes the fitting procedure of the optical potential constants easier. Further, it reflects some dynamical aspects of the $N\bar{N}$ interaction, particularly those associated with isospin effects. The optical model formalism is briefly presented in Sec. III. The resulting parameters of the optical potential are given in Sec. IV. In addition, numerical instabilities are discussed here,

which we observed in solutions of the optical model equations in some cases. The calculated cross sections are compared with the experimental data in Sec. V. A summary is presented in Sec. VI.

II. PARAMETRIZATION OF TOTAL CROSS SECTIONS

There are several parametrizations of total and also differential $N\bar{N}$ cross sections reported earlier. The framework usually used in the low-energy region is the scattering length expansion,[11] which includes also effective ranges in nucleon-antinucleon s and p waves in some cases.[12] Such studies were mainly motivated by the unusual behavior of the real-to-imaginary ratio of the $p\bar{p}$ forward elastic scattering amplitude $\rho = \mathrm{Re}F_{\bar{p}p}/\mathrm{Im}F_{\bar{p}p}$.

Some recent experiments[13,14] seem to indicate that the parameter ρ changes sign in the vicinity of the $p\bar{p} \to n\bar{n}$ threshold. This is the reason why recent work takes into account different thresholds in $p\bar{p}$ and $n\bar{n}$ reactions and incorporates unitarity and analyticity in a proper way.

Both the optical model analysis[6] and effective range expansion study[12] find that the effect of the $n\bar{n}$ threshold is small. Moreover, the work done by Mahalanabis, Pirner and Shibata[12] cast some doubts on the validity of the scattering length plus effective range expansion in the case of low-energy $N\bar{N}$ reactions. In fact, such an approach does not allow one to parametrize the $p\bar{p} \to p\bar{p}$, $p\bar{p} \to n\bar{n}$, and $\bar{n}p \to \bar{n}p$ reaction cross sections simultaneously, and the $\bar{n}p \to \bar{n}p$ data are rather seriously underestimated in Ref. 12. As pointed out by Mahalanabis, Pirner, and Shibata,[12] dynamical singularities in the $N\bar{N}$ amplitudes might be responsible for such a discrepancy. It is well known[5] that, e.g., one-pion exchange dominates the charge-exchange $p\bar{p} \to n\bar{n}$ reaction, and the corresponding singularity may restrict the validity of the scattering length expansion to a very small energy interval.

Following these considerations, we parametrized the total cross sections of the $\bar{p}p \to p\bar{p}$, $p\bar{p} \to n\bar{n}$, and $\bar{n}p \to \bar{n}p$ reactions in terms of simple rational functions as follows:

$$\sigma_{\bar{p}p}^{\mathrm{el}} = \frac{A}{1+\alpha k^2}, \quad \sigma_{\bar{n}p}^{\mathrm{el}} = \frac{B}{1+\beta k^2}, \tag{1a}$$

$$\sigma_{\bar{p}p}^{\mathrm{tot}} = \frac{1}{2}\left[\sigma_0 \frac{1}{1+\alpha' k^2} + \sigma_1 \frac{1}{1+\beta' k^2}\right], \tag{1b}$$

$$\sigma_{\bar{n}p}^{\mathrm{tot}} = \sigma_1 \frac{1}{1+\beta' k^2},$$

$$\sigma_{\bar{p}p}^{\mathrm{CEX}} = \frac{k_f}{k} \frac{C}{(1+\alpha k^2)(1+\gamma k^2)}, \tag{1c}$$

where

$$\sigma_0 = a_0 + b_0/k, \quad \sigma_1 = a_1 + b_1/k. \tag{1d}$$

In Eq. (1c) the factor k_f takes into account the phase space of the final $n\bar{n}$ system and k always means the center-of-mass momentum in the $N\bar{N}$ initial channel. We introduced several (complex) pole terms in Eq. (1), which mimic dynamics singularities in the $N\bar{N}$ amplitudes, rather than to insist on the full treatment of the kinematical cuts associated with the $p\bar{p} \to \bar{n}n$ threshold.

In the numerical fits, a rather complete list of all the experimental total cross sections was included in the laboratory momentum interval $120 \le p_L \le 790$ MeV/c. Two sets of parameters yield an acceptable fit to the 334 data points considered. In obtaining set A, we suppressed the pole terms in σ^{tot} in Eq. (1b) (i.e., $\alpha' \equiv \beta' \equiv 0$), while the complete pole structure of Eq. (1) was considered in the case of set B. The values of the fitted parameters are listed in Table I along with their errors (one standard deviation).

The χ^2 per degree of freedom is 4.06 and 3.22 for fits A and B, respectively. Such large values seem to indicate problems in absolute normalization of some experimental data. This will be demonstrated in Sec. V, where our fitted cross sections and the cross sections calculated using the optical model are compared with experimental data. The inconsistency among different data sets was also the reason why we used fit B as a reference point in our fit of the optical model parameters in Sec. IV.

The parametrizations based on the scattering length expansion are also intended to reproduce $N\bar{N}$ differential

TABLE I. Values of the fitted parameters in Eqs. (1) and (2).

Fit A	Fit B	
$a_0 = 0.147 \pm 0.850$	$a_0 = 14.11 \pm 5.20$	(fm^2)
$b_0 = 21.46 \pm 0.71$	$b_0 = 11.74 \pm 2.23$	(fm)
$a_1 = 12.64 \pm 0.84$	$a_1 = 15.81 \pm 2.29$	(fm^2)
$b_1 = 4.97 \pm 0.66$	$b_1 = 3.70 \pm 0.96$	(fm)
$A = 8.54 \pm 0.15$	$A = 8.51 \pm 0.15$	(fm^2)
$B = 6.62 \pm 1.14$	$B = 6.69 \pm 0.63$	(fm^2)
$C = 2.027 \pm 0.014$	$C = 2.025 \pm 0.014$	(fm^2)
$\alpha = 0.261 \pm 0.015$	$\alpha = 0.259 \pm 0.016$	(fm^2)
$\beta = 0.0971 \pm 0.198$	$\beta = 0.108 \pm 0.082$	(fm^2)
$\gamma = 0.0494 \pm 0.0086$	$\gamma = 0.0506 \pm 0.0090$	(fm^2)
$\alpha' = 0$	$\alpha' = 0.190 \pm 0.140$	(fm^2)
$\beta' = 0$	$\beta' = \beta$	(fm^2)

cross sections, while our ansatz (1) deals with the total cross sections only. Nevertheless, a direct comparison of the two approaches is feasible in the zero-energy limit. Here,

$$\lim_{k\to 0} k\sigma^{\rm tot}_{\bar{n}p}(k) = -4\pi\,{\rm Im}\lambda_1 \ ,$$
$$\lim_{k\to 0} k\sigma^{\rm tot}_{\bar{p}p}(k) = -2\pi({\rm Im}\lambda_0 + {\rm Im}\lambda_1) \ , \tag{2}$$

where λ_0 and λ_1 are the spin-averaged (complex) s-wave scattering lengths in the isospin states $I=0$ and 1, respectively. The quantities ${\rm Im}\lambda_1$ as obtained from our fits A and B are compared with the results of the scattering length expansion work[12] in Table II.

Similarly, in the zero-energy limit, we have

$$\sigma^{\rm el}_{\bar{n}p}(0) = 4\pi|\lambda_1|^2, \quad \sigma^{\rm el}_{\bar{p}p}(0) = \pi|(\lambda_0+\lambda_1)|^2 \ . \tag{3}$$

This allows us to extract the quantity $|{\rm Re}(\lambda_0+\lambda_1)|$. In such a way, predictions for $|\Delta E_{1s}|$ and Γ_{1s} can be obtained from our fits making use of the familiar relation between $1s$-state scattering lengths and $1s$-level energy shift and width of the antiprotonic hydrogen:

$$\Delta E_{1s} - i\Gamma_{1s}/2 = \frac{2}{a_B^3 m_p}(\lambda_0+\lambda_1) \ , \tag{4}$$

where m_p is the proton mass and $a_B = 57.6$ fm is the Bohr radius of the $1s$ orbit. The procedure is, however, meaningful only when the spin singlet and spin triplet scattering length differ not too much.

The results obtained for $|\Delta E_{1s}|$ and Γ_{1s} in our fits and that of Ref. 12 are compared in Table II with experimental data. Additional information concerning the number of fitted points, χ^2 per degree of freedom, and laboratory momentum interval of the fitted data is also given in Table II.

It should be noted that $|{\rm Re}(\lambda_0+\lambda_1)|^2$ turns out to be negative in the case of our fit A and also Γ_{1s} is too large in comparison with the experiment. Therefore, our fit A provides a rather poor extrapolation toward the elastic threshold.

Fit A of Ref. 12, which is based on the scattering length expansion, does not reproduce the level shift very well in spite of the fact that the atomic data were included into the fitted quantities.

Our fit B reproduces well the $N\bar{N}$ total cross sections in a large interval of beam momenta, and it also provides a very reasonable extrapolation toward the antiprotonic hydrogen. It can be concluded that a sufficiently rich pole structure in expressions for $\sigma^{\rm tot}$, $\sigma^{\rm el}$, and $\sigma^{\rm CEX}$ is vital for obtaining a good fit to the experimental data in the interval of beam momenta 0–700 MeV/c.

Our fit B predicts also a rather strong dependence of scattering length on isospin. As a measure of this dependence, the ratio

$$R = \frac{2\,{\rm Im}\lambda_1}{{\rm Im}\lambda_0 + {\rm Im}\lambda_1} \tag{5}$$

is sometimes introduced.[9] The $N\bar{N}$ annihilation is represented in most optical model calculations by an empirical isoscalar term. Such calculations usually predict the ratio R much closer to unity in comparison with our values as given in Table II. This may indicate the necessity of introducing an isovector annihilation term into the optical potential in addition to the isoscalar one. Our value of $R=0.48$ is rather close to values obtained for antiproton annihilation by helium isotopes (for a review of recent data on R, see Ref. 9), where the role of p- and d-wave processes is also important. Our fit B may be consistent with these data, if the annihilation depends rather strongly on isospin, but only weakly on orbital momentum.

III. MOMENTUM SPACE RELATIVISTIC OPTICAL MODEL

Following closely the philosophy of the Bonn meson-exchange model, we constructed our $N\bar{N}$ optical potential in the framework of the relativistic three-dimensional Blankenbecker-Sugar (BbS) reduction of the Bethe-Salpeter (BS) equation. The procedure consists of replacing in the BS equation the relativistic two-nucleon propagator by the covariant three-dimensional one that sets the time component of the intermediate relative momentum to zero.[15] In the following it is suitable to introduce the

TABLE II. Scattering lengths and $1s$-level shifts and widths. Ratio R is defined by Eq. (5).

	Fit A	Fit B	Fit A of Ref. 12	Exp. data Ref. 43
${\rm Im}\lambda_0$ (fm)	−1.71	−0.93	−0.9	−1.07±0.16
${\rm Im}\lambda_1$ (fm)	−0.39	−0.29	−0.5	−0.83±0.07
$\lvert\Delta E_{1s}\rvert$ (keV)	negative	0.48	0.087	0.70±0.07
Γ_{1s} (keV)	1.83	1.07	1.22	1.20±0.14
R	0.376	0.480	0.714	0.87±0.11
No. of data points	334	334	163	
χ^2/d.f.	4.06	3.22	4.4	
Laboratory momentum range (MeV/c)	120–790	120–790	0–300	
No. of fitted parameters	10	11	12	

"minimal relativity" factors by definition:

$$V(\mathbf{q}',\mathbf{q})=-(m/4\pi)\sqrt{m/E_{q'}}\,\bar{V}(\mathbf{q}',\mathbf{q})\sqrt{m/E_q}\ , \tag{6}$$

where $E_q=\sqrt{m^2+q^2}$, m is the average nucleon mass, and the analogous expression applies for the invariant amplitude. Then the matrix elements of the scattering amplitude $F(\nu\mathbf{q}'_\nu,\mu\mathbf{q}_\mu)$ calculated between physical states satisfy the equation

$$F(\nu\mathbf{q}'_\nu,\mu\mathbf{q}_\mu)=V(\nu\mathbf{q}'_\nu,\mu\mathbf{q}_\mu) - \frac{2}{(2\pi)^2}\int d^3k\sum_\eta \frac{V(\nu\mathbf{q}'_\nu,\eta\mathbf{k})F(\eta\mathbf{k},\mu\mathbf{q}_\mu)}{q_\mu^2-k^2+i\varepsilon}\ , \tag{7}$$

which is formally identical with the Lippman-Schwinger (LS) equation. In Eq. (7), ν, μ, and η denote the channel numbers in the $\bar{p}p$ scattering. There are two coupled channels: the elastic channel ($\nu=1$) and the charge-exchange one ($\nu=2$). The absolute values of the channel momenta q_μ, $\mu=1$, or 2, differ because we assume a mass splitting between the neutron and proton, and therefore we also include in this way the threshold effect associated with opening of the charge-exchange channel. The numerical solution of Eq. (7) was performed in the usual LSJ basis using the matrix inversion method.

The optical potential $\bar{V}$ in Eq. (6) consists of the diffractive (U) and absorptive (W) terms:

$$\bar{V}=U+iW\ . \tag{8}$$

In the case of $\bar{N}N$ interaction, the long- and intermediate-range parts of U are supposed to be represented mainly by meson exchanges such as in the successful models of NN interaction (Bonn, Paris). The connection between the NN meson-exchange potential and the diffractive part of the $\bar{N}N$ interaction is then carried by the G-parity transformation. As far as the short-range part of U is concerned, there is no belief that the meson-exchange picture is of any relevance. The nucleon and antinucleon cores start to overlap at $r\leq 0.8$ fm, and a much more complicated dynamical picture is expected to evolve there. The corresponding short-ranged part of the NN potential is usually regularized in terms of form factors. However, there is no guide as to how to carry out the transition from the NN to $\bar{N}N$ interaction in such a case. This is the reason why a phenomenological form is usually chosen for the short-range part of U. This piece of the $\bar{N}N$ interaction is, however, not expected to play any significant role in the $\bar{N}N$ scattering, since the annihilation potential W provides a strong damping of the $\bar{N}$-N wave function at short relative distances.

In our work we started from the relativistic static one-meson-exchange parametrization of the full Bonn model in q space (OBEPQ).[15] Performing the G-parity transformation, we have

$$U=\sum_\alpha G_\alpha V_\alpha(\mathrm{OBE})\ , \tag{9}$$

where $\alpha=\pi,\eta,\omega,\rho,\sigma,\delta$ and G_α is the G parity of mesons ($G_\alpha=+1,-1$). Explicit formulas for traditional one-boson-exchange diagrams V_α(OBE) are given in Appendix E.2, in Ref. 15. All the meson parameters as well as the short-range part of V_α(OBE) are kept unchanged. From numerical reasons, however, an additional cutoff was used in our $N\bar{N}$ calculations. The motivation for introducing it and its shape are discussed in Sec. IV.

Recently, there have been several attempts to account for the $\bar{N}N$ annihilation in terms of quark-exchange and annihilation processes (see, e.g., Ref. 16). In view of the prospective application of our model in $\bar{N}$-nucleus calculations, we prefer to introduce a phenomenological form of W with the aim of reproducing as many $\bar{N}N$ experimental data as possible and also to get an insight into the isospin content of the $\bar{N}N$ interaction.

The $\bar{N}N$ annihilation is also expected to induce some dispersive terms in the optical potential (8). It has been shown in Ref. 8 that such terms influence the physical observables to a minimal extent. The only exception is the vector polarizations in $\bar{N}N$ elastic scattering, where some sensitivity can be seen. Measurements of spin observables in $\bar{N}N$ reactions are rather scarce yet and do not allow one to distinguish between the dispersive terms and spin- and/or orbital-momentum-dependent terms of W (for more details see the discussion in Sec. V). This is the reason why we neglect the contribution of induced dispersive terms in our calculations and neglect also any possible dependence of W on spin and orbital momentum. As already mentioned before, the difference between measured $\bar{p}p$ and $\bar{n}p$ data motivated us to suppose the isospin dependence of W.

The volumelike form of the absorptive potential W was tested in our work. Let

$$W=\delta_{I0}W_0+\delta_{I1}W_1\ , \tag{10}$$

where I denotes the total isospin of the $\bar{N}N$ system. Then the radial function is

$$W_j=-w_j\exp(-x_j^2),\quad j=0,1\ . \tag{11}$$

Here, $x_j=\alpha_j r$. The parameters of the model, w_j and α_j, were fitted independently for $I=1$ and 0. In discussing the strength of isospin effects, another form of W can be useful:

$$W=G_1+\tau_1\cdot\tau_2 G_2\ , \tag{12}$$

where

$$G_1=\tfrac{1}{4}(W_0+3W_1)\ ,$$

$$G_2=\tfrac{1}{4}(W_1-W_0)$$

and τ_j, $j=1,2$, are Pauli matrices.

All (static) Coulomb effects were taken into account in our calculations using the prescription by Vincent and Pathak.[17]

IV. FITTING THE PARAMETERS OF THE MODEL

In fitting the parameters α_j and w_j, $j=0$, and 1, we encountered rather serious problems associated with an instability of numerical solutions of Eq. (7) in some cases. The problem deserves a more detailed discussion.

The potential U [Eq. (9)] receives a contribution from nucleon recoil terms (so-called velocity-dependent terms), which remain constant in the limit $q'=q\to\infty$. Therefore the kernel of integral equation (7) without the minimal relativity factors [Eq. (6)], which is formally identical with the case of a nonrelativistic version of the potential OBEPQ, is not of Fredholm type. Even when such factors are introduced, the resulting potential $V(\mathbf{q}',\mathbf{q})$ in Eq. (6) falls off very slowly along the line $q'=q\to\infty$. This is one of the reasons why the solution of Eq. (7) may depend rather strongly on the number of Gaussian mesh points (N) being used and an additional cutoff is necessary.

In the case of N-N scattering, numerical stability can be achieved using a moderate number of Gaussian mesh points ($30\le N\le 50$). On the other hand, the solution obtained for the N-$\bar{N}$ amplitudes becomes increasingly unstable with decreasing strength w_j, $j=0$, 1, of the annihilation potential. The reason is rather obvious. The ω-meson exchange produces a strong attractive contribution to the real part of the N-$\bar{N}$ scalar potential, and many N-$\bar{N}$ bound states occur in the limit $\omega_j=0$. In such a case, a large number[18] of mesh points is needed ($N\simeq 90$) to obtain a numerically stable result. However, this approach seems to be rather unpractical in view of future applications of our model.

This is the reason why we applied an additional cutoff to the OBE part of the $N\bar{N}$ potential U [see Eq. (9)]:

$$U(\mathbf{q}',\mathbf{q})\to\frac{1}{1+(q'/\Lambda)^{10}}U(\mathbf{q}',\mathbf{q})\frac{1}{1+(q/\Lambda)^{10}}\ . \tag{13}$$

The procedure was earlier used by Maruyama, Furui, and Faessler[19] and provides a very strong damping of the short-range attraction in the $N\bar{N}$ potential, leaving the long- and medium-range properties of $U(\mathbf{q}',\mathbf{q})$ almost intact. The choice of the cutoff momentum $\Lambda=2.0$ GeV leaves the NN results unchanged[20] and ensures at the same time a numerical stability of $N\bar{N}$ amplitudes even when a moderate number of mesh points is used.

In fitting the parameters of our models, we used the parametrization of $N\bar{N}$ total cross sections [Eqs. (1)] (fit B) at several energies as quasiexperimental data. The best-fit values of parameters α_i and w_j were found to be

$$\begin{aligned}&\alpha_1=1.47\ \text{fm}^{-1},\quad w_1=0.6\ \text{GeV}\ ,\\ &\alpha_0=1.80\ \text{fm}^{-1},\quad w_0=3.0\ \text{GeV}.\end{aligned} \tag{14}$$

In Sec. V it will be shown that the model accounts for $N\bar{N}$ observables quite well. Equation (14) seems to indicate that the isospin dependence of the $N\bar{N}$ annihilation is very strong. Really, the $N\bar{N}$ annihilation potential in the $I=0$ channel turns out to be much smaller than that in the $I=1$ channel. However, one has to emphasize that the parameters α_j and w_j are strongly correlated. There is a valley in the χ^2 plane of both the parameters α_0, w_0 and also α_1, w_1. In the vicinity of the points given by (14), the bottom of each valley can be described approximately by the line

$$\alpha_j=d_j w_j+c_j,\quad j=0,1\ , \tag{15}$$

where $d_0=0.13$ GeV^{-1}fm^{-1}, $d_1=0.5$ GeV^{-1}fm^{-1}, $c_0=1.41$ fm^{-1}, and $c_1=1.17$ fm^{-1}. Therefore, the increasing range of the annihilation potential (decreasing α_j) can be compensated to a large extent by the decreasing strength w_j in each isospin channel $j=0$ and 1. We can conclude that the existing experimental data do not allow one to determine the absolute minimum of χ^2 very accurately. It is also interesting to note that the $p\bar{p}$ scattering length is the observable, which requires as large a value of w_0 as $w_0=3.0$ GeV. If the scattering length were not included into the set of fitted experimental data, the difference between w_0 and w_1 would be much smaller.

It is also instructive to estimate the strength of the isovector term G_2 in Eq. (12) in comparison with the isoscalar G_1 one. In coordinate space the ratio

$$\varepsilon(r)=\frac{G_2}{G_1}=\frac{W_1-W_0}{W_0+3W_1} \tag{16}$$

increases monotonically. It starts from $\varepsilon(0)=-0.5$, changes sign at $r\simeq 1.2$ fm, and reaches the value $\varepsilon(\infty)=\frac{1}{3}$. Except for the regions $r\le 0.6$ fm or $r\ge 1.6$ fm, where the relative $N\bar{N}$ wave function or the annihilation potential tend to vanish, $\varepsilon(r)$ is close to zero. Therefore, the isospin effects in $N\bar{N}$ or $\bar{N}$-nucleus scattering and annihilation are expected to be much weaker than the difference between w_0 and w_1 [Eqs. (14)] seems to indicate.

V. DISCUSSION

Using the optical model [Eqs. (6)–(13)] and fitted parameters [Eq. (14)], which characterize our phenomenological annihilation potential, we calculated various observables in $N\bar{N}$ scattering and annihilation. In this section a comparison is made between the calculated results and corresponding experimental data.

In the case of $N\bar{N}$ total and total elastic cross sections, the results obtained using our empirical formulas (1) are also shown. These results were obtained using the set of parameters denoted as "fit B" in Table I.

In Figs. 1 and 2 the $\bar{p}p$ elastic differential cross sections are compared with the experimental data at two energies. We can conclude that our optical model accounts for the data quite well. Our model works equally well in the whole region of scattering momenta considered, $100\le p_L\le 1000$ MeV/c.

The vector polarization P in $\bar{p}p$ elastic scattering is shown in Fig. 3 at momenta 523, 670, and 700 MeV/c. The trend of the experimental data is reproduced quite well by our optical model, and the dip in P also seems to occur at the correct position. However, our model underestimates the data systematically at low scattering angles ($\vartheta\le 90°$). Of course, one could include a phenomenological spin-dependent term into our annihilation potential and try to obtain a better fit (see, e.g., Ref. 2). In fact, a recent study[21] of level ordering $\bar{p}$-^{174}Yb atoms indicates strongly the presence of such terms. On the other hand, the discrepancies observed in Fig. 3 cannot be uniquely interpreted as a manifestation of spin terms in the annihilation potential, since P was shown to depend

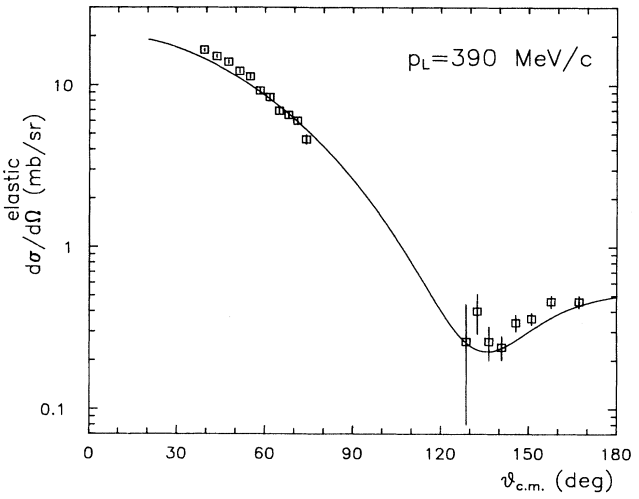

FIG. 1. Calculated (OM) differential cross section of elastic $\bar{p}p$ scattering. Experimental data are from Ref. 24.

rather strongly[2] also on the radial shape of the scalar annihilation potential (10). Our experience is the same.

Moreover, it has been observed in Ref. 8 that the two meson-exchange contributions, particularly 2π and $\pi\rho$, to the diffractive part of the optical potential (8) influence P rather strongly, too. The measurements of vector polarization and spin-transfer coefficients in $p\bar{p}$ elastic and charge-exchange scattering, which are already finished or which are now under way on LEAR,[22] will hopefully allow one to determine the spin content of the annihilation potential and also to learn more about the dispersive corrections to it.

Differential charge-exchange cross sections at momenta 390 and 590 MeV/c are shown in Fig. 4. Our model predicts a "dip-bump" structure in the cross sections, at

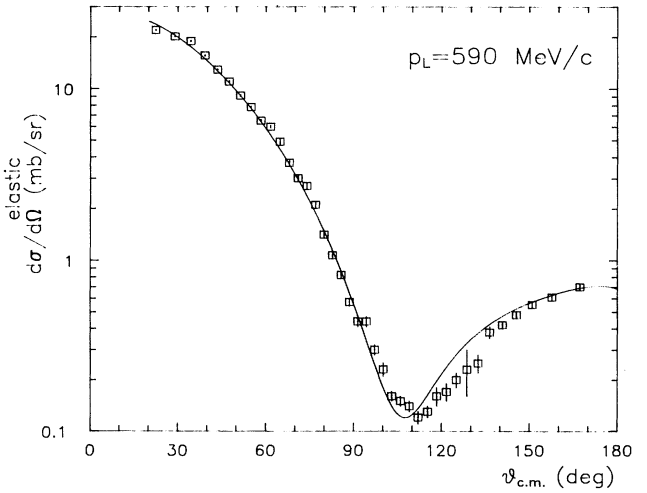

FIG. 2. Calculated (OM) differential cross section of elastic $\bar{p}p$ scattering. Experimental data are from Ref. 24.

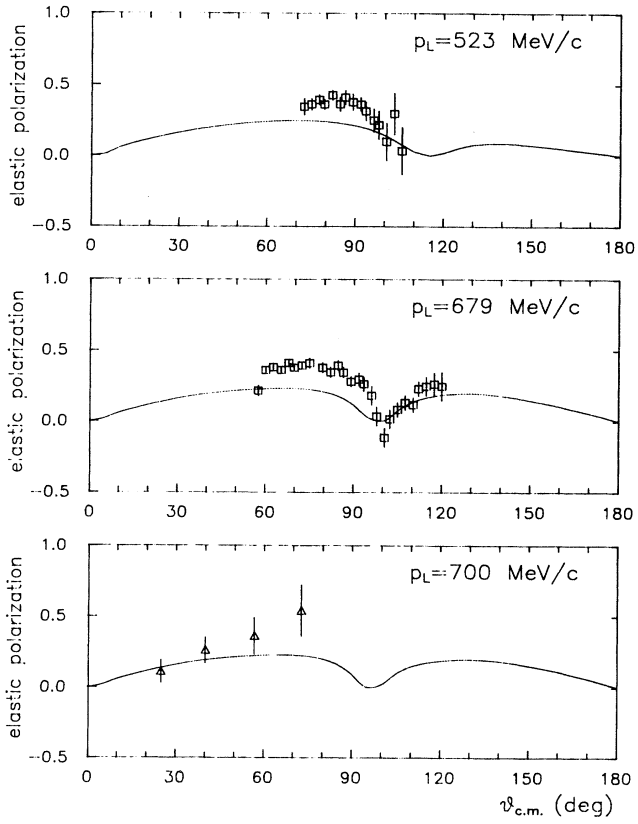

FIG. 3. The vector polarization P in elastic $\bar{p}p$ scattering. The experimental data are from Refs. 25 and 26.

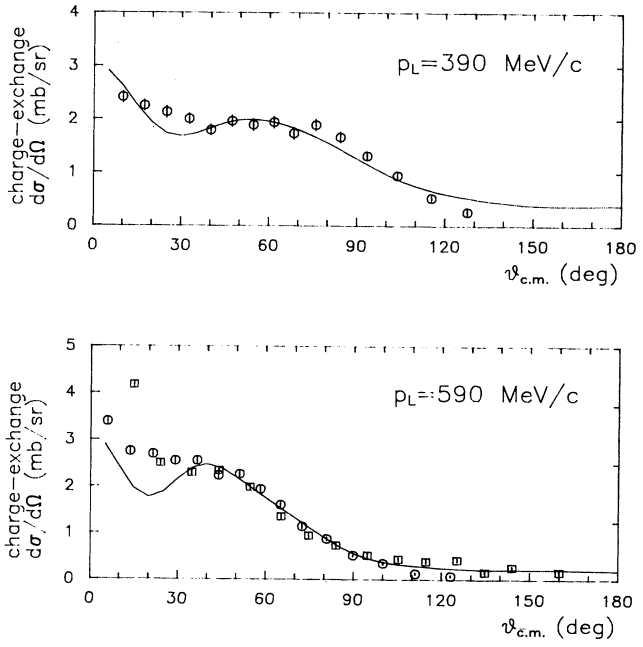

FIG. 4. Comparison of experimental (Refs. 27 and 28) and calculated (OM) differential cross sections for the $\bar{p}p \rightarrow \bar{n}n$ reaction.

variance with experiment, which requires a much less pronounced structure, if any. The disagreement is more serious at $p_L = 590$ Mev/c. Such an unrealistic "dip-bump" structure typically occurs in models based on Bonn[8] or Paris[7] potentials, while the Nijmegen[1] potential does not produce any dip and accounts for the experimental data well. However, it would be premature to interpret the disagreement seen in Fig. 4 as a failure of the Bonn (or Paris) potential, since the forward $\bar{p}p \to \bar{n}n$ differential cross section was shown to be very sensitive to the shape of both the real[8] and imaginary[2] parts of the optical potential.

The $p\bar{p}$ total, total elastic, and charge-exchange cross sections are shown in Fig. 5. A comparison is made between our optical model predictions, the calculations based on the empirical formulas (1), and experimental data. We can conclude that both the empirical formulas and optical model reproduce the data well. Only the optical model underestimates slightly the experimental σ^{tot} around $T_L = 50$ MeV.

A similar comparison was made in Fig. 6 in the case of $\bar{n}p$ total and annihilation cross sections. The annihilation cross section is again reproduced very well. The calculations based on the optical model and empirical formulas

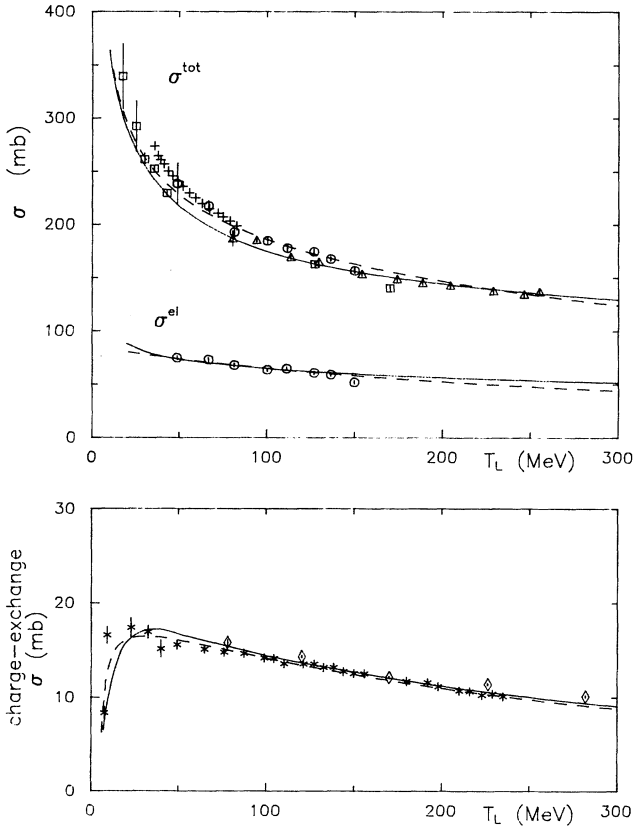

FIG. 5. Comparison of experimental and calculated total, total elastic and total charge-exchange $\bar{p}p$ cross sections ($\sigma^{\text{tot}}, \sigma^{\text{el}}, \sigma^{\text{CEX}}$). The solid and dashed lines denote the results obtained using the optical model and fit B, respectively. Experimental data are from Refs. 29–33 and Ref. 24.

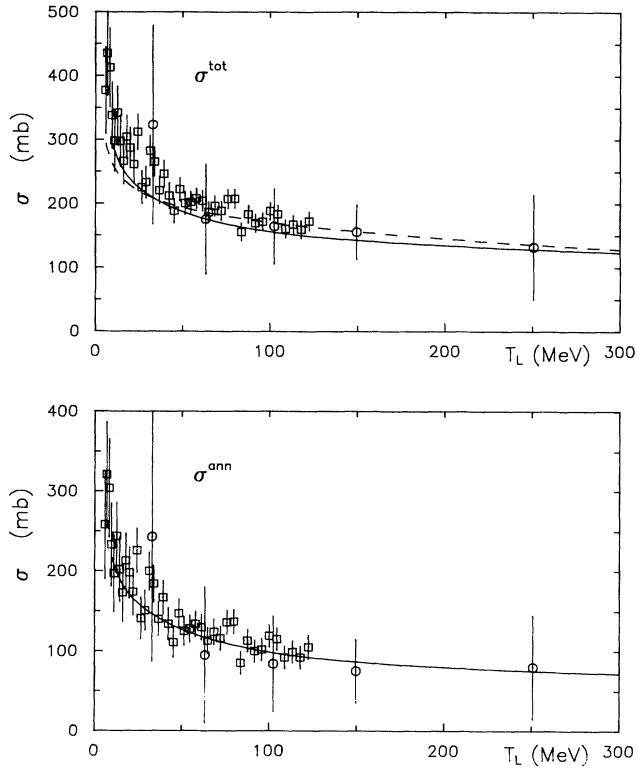

FIG. 6. Comparison of experimental and calculated total and annihilation $\bar{n}p$ cross section ($\sigma^{\text{tot}}, \sigma^{\text{ann}}$). The meaning of the curves is the same as in Fig. 5. The data are from Refs. 34 and 35.

underestimate slightly σ^{tot} at low reaction energies; however, the experimental data have large errors there.

The backward elastic differential cross is shown in Fig. 7 for $p\bar{p}$ scattering as a function of the scattering momentum. The optical model prediction reproduces the experimental data quite well. The only exception is the peak region at $p_L \simeq 500$ MeV/c, where the model somewhat underestimates the data.

The real-to-imaginary ratio of the $p\bar{p}$ forward elastic scattering amplitude ρ is shown in Fig. 8. The optical model underestimates the data in the whole region of the scattering momenta considered and does not reproduce the structure seen in the data around $p_L = 200$ MeV/c at

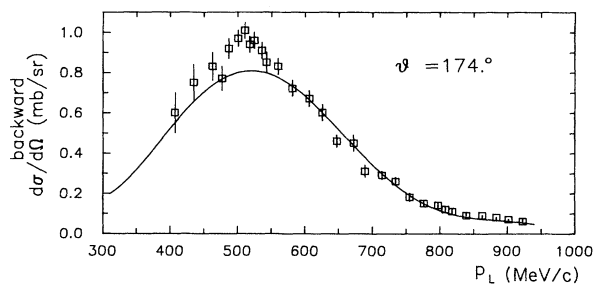

FIG. 7. Calculated (OM) backward differential cross section for $\bar{p}p$ elastic scattering. The data are from Ref. 36.

all. The value of ρ at zero p_L is lower than that obtained from $\bar{p}$-atom experiments.

Studies done within the effective range approximation[12] reveal that ρ receives repulsive s-wave and attractive p-wave contributions in the low-energy region. The p-wave contribution, being sufficiently strong, is peaked at $p_L = 100$ MeV/c and can cause the ratio ρ to be positive there.

Adopting this point of view, we can conclude that the p-wave interaction as predicted by the optical model is too weak in the low-energy region. There are at least two mechanisms which can lead to a stronger p-wave interaction in $p\bar{p}$ scattering. First, the two meson exchanges are expected to give rather important contributions[8] to the optical potential. Second, the $p\bar{p}$ annihilation gives rise to spin-dependent terms in the optical potential, which can, as, e.g., the spin-orbit term, enhance the p-wave interaction leaving the s-wave interaction unchanged.

It is tempting to try to account simultaneously for the discrepancies observed in P and ρ as well as the anomalous level ordering in $\bar{p}$-^{174}Yb atoms just by introducing a spin-orbit interaction term in the optical potential associated with the $p\bar{p}$ annihilation. Corresponding calculations are in progress. Needless to say, more polarization $p\bar{p}$ experiments would be helpful.

In Table III a comparison is made between the calculated scattering lengths and corresponding experimental data. Our optical model seems to underestimate somewhat both the real and imaginary part (in absolute value) of $\lambda_{\bar{p}p}$ and also the imaginary part of $\lambda_{\bar{n}p}$. However, the experimental average $\lambda_{\bar{p}p}$ as given in Table III receives contributions also from measurements that yield smaller $\mathrm{Re}\lambda_{\bar{p}p}$ than, and almost the same $\mathrm{Im}\lambda_{\bar{p}p}$ as, our calculated results (for a review of the experimental $\lambda_{\bar{p}p}$, see, e.g., Ref. 23). It is difficult to arrive at more definite conclusions here.

Our predictions for the ratio R [Eq. (5)] reproduce the experiment reasonably well. It it somewhat surprising that R turns out to be very close to unity in spite of the fact that the strength of the annihilation potential is very different in the $I=0$ and 1 channels [see Eq. (14)]. Such low values of R as obtained in Table II using the empirical parametrizations are not supported by the optical model calculations. Even when the strength w_0 of the $I=0$ optical potential is changed along the line (15) down to 2 GeV, the ratio R remains close to unity.

V. SUMMARY

Experimental total, annihilation, and total scattering cross sections for $p\bar{p} \to p\bar{p}$, $p\bar{p} \to n\bar{n}$, and $\bar{n}p \to \bar{n}p$ reactions were parametrized in terms of rational functions. Good agreement with experiment was reached in the laboratory momentum interval 0–800 MeV/c. Using this parametrization as quasiexperimental data, we fitted the parameters of an isospin-dependent annihilation component of the effective (optical) $N\bar{N}$ potential. In the fitting procedure, the real part of the effective potential was fixed to be the G-parity transform of the relativistic static Bonn NN potential (OBEPQ).

The resulting effective potential yields a good description of differential and total $N\bar{N}$ cross sections, and $\bar{p}$-atom level shift and width as well. The model reproduces rather well also the charge-exchange $p\bar{p} \to n\bar{n}$ differential cross sections and polarization in elastic $p\bar{p}$ scattering. The real-to-imaginary ratio ρ of the $p\bar{p}$ forward elastic scattering amplitude as obtained from our model disagrees with the experimental data, and this long-standing puzzle is evidently not associated with isospin effects.

The fitting parameters of the optical model (strength and radius of the imaginary part of the optical potential) turn out to be very different in either isospin channel; however, the parameters are strongly correlated.

Numerical instabilities are also discussed, which arise in some regions of the fitting parameters.

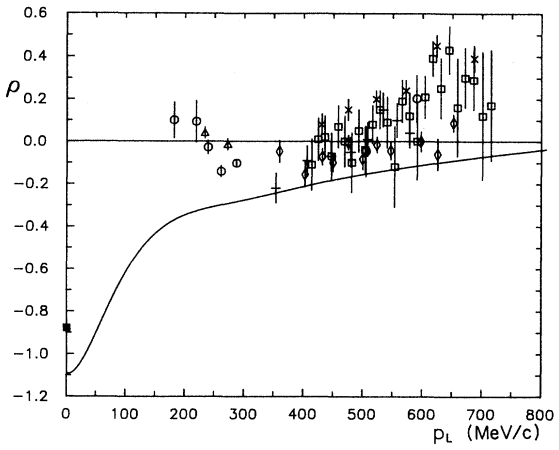

FIG. 8. The ratio ρ of real to imaginary parts of the forward amplitude for $\bar{p}p$ scattering as a function of laboratory momentum p. Comparison of theoretical predictions (OM) and experimental data of Refs. 37–42 and Ref. 31.

TABLE III. Spin-averaged scattering lengths calculated from our optical model (OM). Ratio R is defined by Eq. (5).

	OM	Expt. data (Refs. 23 and 43)
$\lambda_{\bar{p}p}$ (fm)	$0.82-i0.67$	$0.93\pm0.09-i(0.95\pm0.12)$
$\lambda_{\bar{n}p}$ (fm)	$0.71-i0.65$	$0.96\pm0.25-i(0.83\pm0.07)$
$\mathrm{Im}\lambda_0$ (fm)	-0.69	-1.07 ± 0.16
R	0.97	0.87 ± 0.11

ACKNOWLEDGMENTS

One of the authors (R.M.) profited from numerous discussions with members of Graz group and particularly with W. Plessas. He also acknowledged inspiring conversations with C. Guaraldo and the hospitality extended to him at INFN during the final stage of the work. The authors are indebted to R. Machledit for providing them with the numerical code of the Bonn potential.

[1]G. Q. Liu and F. Tabakin, Phys. Rev. C **41**, 665 (1990); D. H. Timmers, W. A. Saden, and J. J. deSwart, Phys. Rev. D **29**, 1928 (1984).

[2]T. Ueda, Prog. Theor. Phys. **62**, 1670 (1979); in *Proceedings of the INS International Symposium on Hypernuclear Physics,* Tokyo, 1986, edited by H. Bando, O. Hoshimoto, and K. Ogawa (Institute for Nuclear Study, Tokyo, 1986), p. 344.

[3]T. Mizutani, F. Myhrer, and R. Tegen, Phys. Rev. D **32**, 1663 (1985).

[4]M. Kohno and W. Weise, Nucl. Phys. **A454**, 429 (1986).

[5]T. A. Shibata, Phys. Lett. B **189**, 232 (1987).

[6]B. Moussallam, Z. Phys. A **325**, 1 (1986).

[7]C. Cõté, M. Lacombe, B. Loisean, B. Moussallam, and R. Vint, Phys. Rev. Lett. **48**, 1319 (1982).

[8]T. Hippchen, K. Holinde, and W. Plessas, Phys. Rev. C **39**, 761 (1989).

[9]F. Balestra *et al.*, Nucl. Phys. **A491**, 572 (1989).

[10]A. Angelopoulos, Phys. Lett. B **212**, 129 (1988).

[11]B. O. Kerbikov and Yn. A. Simonov, Phys. Lett. B **208**, 309 (1988); A. E. Kudrjavtsev and V. E. Markushin, Institute of Theoretical and Experimental Physics (ITEP) Report No. 179 (1985).

[12]J. Mahalanabis, H. J. Pirner, and T. A. Shibata, Nucl. Phys. **A485**, 546 (1988).

[13]S. Ahmad *et al.*, Phys. Lett. **157B**, 333 (1985).

[14]T. P. Gorringe *et al.*, Phys. Lett. **162B**, 71 (1985).

[15]R. Machleidt, K. Holinde, and Ch. Elster, Phys. Rep. **149**, 1 (1987).

[16]A. M. Green and J. A. Niskanen, Nucl. Phys. **A412**, 448 (1984); S. Furui and A. Faessler, *ibid.* **A424**, 525 (1984).

[17]C. M. Vincent and S. S. Phatak, Phys. Rev. C **10**, 391 (1974).

[18]R. Machleidt, private communication.

[19]M. Maruyama, S. Furui, and A. Faessler, Nucl. Phys. **A472**, 643 (1987).

[20]J. Haidenbauer, private communication.

[21]S. Wycech, H. Poth, and J. R. Rook, Z. Phys. A **335**, 355 (1990).

[22]R. Birsa *et al.*, Report No. CERN-EP/90-68 (1990); C. Guaraldo, private communication.

[23]L. S. Pinsky, in *Proceedings of the Fourth LEAR Workshop,* Villars-sur-Ollon, Switzerland, 1987, edited by C. Amsler, G. Backenstoss, R. Klapisch, C. Leluc, D. Simon, and L. Tauscher (Harwood, Academic, Chur, 1988), p. 263.

[24]T. Kageyama, T. Fujii, K. Nakamura, F. Sai, S. Sakamoto, S. Sato, T. Takahashi, T. Tanimori, S. S. Yamamoto, and Y. Takada, Phys. Rev. D **35**, 2655 (1987).

[25]M. Kimura *et al.*, Nuovo Cim. **71A**, 438 (1982).

[26]R. A. Kunne *et al.*, Phys. Lett. B **206**, 557 (1988).

[27]K. Nakamura, T. Fujii, T. Kageyama, F. Sai, S. Sakamoto, S. Sato, T. Takahashi, T. Tanimori, S. S. Yamamoto, and Y. Takada, Phys. Rev. Lett. **53**, 885 (1984).

[28]W. Bruckner *et al.*, Phys. Lett. **169B**, 302 (1986).

[29]K. Nakamura *et al.*, Phys. Rev. D **29**, 349 (1984).

[30]V. Chaloupka *et al.*, Phys. Lett. **61B**, 487 (1976).

[31]W. Bruckner *et al.*, Phys. Lett. **158B**, 180 (1985).

[32]D. V. Bugg *et al.*, Phys. Lett. B **194**, 563 (1987).

[33]R. P. Hamilton, T. P. Pun, R. D. Tripp, H. Nicholson, and D. M. Lazarus, Phys. Rev. Lett. **44**, 1179 (1980).

[34]T. Armstrong *et al.*, Phys. Rev. D **36**, 659 (1987).

[35]B. Gunderson, J. Learned, J. Mapp, and D. D. Reeder, Phys. Rev. D **23**, 587 (1981).

[36]M. Alston-Garnjost, R. P. Hamilton, R. W. Kenney, D. L. Pollard, R. D. Tripp, H. Nicholson, and D. M. Lazarus, Phys. Rev. Lett. **43**, 1901 (1979).

[37]V. Ashford, M. E. Sainio, M. Sakitt, J. Skelly, R. Debbe, W. Fickinger, R. Marino, and D. K. Robinson, Phys. Rev. Lett. **54**, 518 (1985).

[38]L. Linssen *et al.*, Nucl. Phys. **A469**, 726 (1987).

[39]H. Iwasaki *et al.*, Phys. Lett. **103B**, 247 (1981).

[40]M. Cresti, L. Peruzzo, and G. Sartori, Phys. Lett. **132B**, 209 (1983).

[41]M. Ziegler *et al.*, Phys. Lett. B **206**, 151 (1988).

[42]H. Iwasaki *et al.*, Nucl. Phys. **A433**, 580 (1985).

[43]G. S. Mutchler *et al.*, Phys. Rev. D **38**, 742 (1988).